Rotational effects in the band oscillator strengths and predissociation linewidths for the lowest u 1 – X g + 1 transitions of N 2

V. E. Haverd, B. R. Lewis, S. T. Gibson, and G. Stark

Citation: The Journal of Chemical Physics **123**, 214304 (2005); doi: 10.1063/1.2134704
View online: http://dx.doi.org/10.1063/1.2134704
View Table of Contents: http://scitation.aip.org/content/aip/journal/jcp/123/21?ver=pdfcov
Published by the AIP Publishing

Rotational effects in the band oscillator strengths and predissociation linewidths for the lowest $^1\Pi_u - X\,^1\Sigma_g^+$ transitions of N_2

V. E. Haverd,[a] B. R. Lewis,[b] and S. T. Gibson
Research School of Physical Sciences and Engineering, The Australian National University, Canberra, Australian Capital Territory 0200, Australia

G. Stark
Department of Physics, Wellesley College, Wellesley, Massachusetts 02481

(Received 2 September 2005; accepted 12 October 2005; published online 2 December 2005)

A coupled-channel Schrödinger equation (CSE) model of N_2 photodissociation, which includes the effects of all interactions between the b, c, and o $^1\Pi_u$ and the C and C' $^3\Pi_u$ states, is employed to study the effects of rotation on the lowest-v $^1\Pi_u - X\,^1\Sigma_g^+(v,0)$ band oscillator strengths and $^1\Pi_u$ predissociation linewidths. Significant rotational dependences are found which are in excellent agreement with recent experimental results, where comparisons are possible. New extreme-ultraviolet (EUV) photoabsorption spectra of the key $b\,^1\Pi_u \leftarrow X\,^1\Sigma_g^+(3,0)$ transition of N_2 are also presented and analyzed, revealing a $b(v=3)$ predissociation linewidth peaking near $J=11$. This behavior can be reproduced only if the triplet structure of the C state is included explicitly in the CSE-model calculations, with a spin-orbit constant $A \approx 15$ cm^{-1} for the diffuse $C(v=9)$ level which accidentally predissociates $b(v=3)$. The complex rotational behavior of the $b-X(3,0)$ and other bands may be an important component in the modeling of EUV transmission through nitrogen-rich planetary atmospheres. © *2005 American Institute of Physics*.
[DOI: 10.1063/1.2134704]

I. INTRODUCTION

There has recently been a reawakening of interest in the extreme-ultraviolet (EUV) spectroscopy and predissociation dynamics of molecular nitrogen, prompted largely by their importance in understanding the radiative transfer and photochemistry of nitrogen-rich planetary atmospheres. For example, accurate knowledge of the EUV spectroscopy of N_2 is required for the correct interpretation of solar occultations such as those associated with the current encounters of Titan by Cassini and also for radiative transfer models used to interpret upper atmospheric airglow observations. As noted by Stark *et al.*,[1] who provide a comprehensive review of previous work, N_2 spectroscopic models used for such purposes in the EUV require a complete knowledge of line positions, oscillator strengths, and widths, including rotational effects.

The first dipole-allowed transitions of N_2 occur in the $\gtrsim$101 000 cm^{-1} region, accessing the strongly coupled valence and Rydberg states of $^1\Pi_u$ and $^1\Sigma_u^+$ symmetries.[2,3] Recently, linewidths and/or lifetimes for the lowest of these states have been characterized experimentally for the $^{14}N_2$, $^{15}N_2$, and $^{14}N\,^{15}N$ isotopomers by Sprengers *et al.*,[4–6] while oscillator strengths and some linewidths have been measured by Stark *et al.*,[1] including, for the first time for these transitions, quantification of rotational dependences. These new results have considerably improved the experimental database for N_2 and have thereby supported the development of the first quantitative model of N_2 predissociation, by Lewis *et al.*,[7] who considered specifically the rotationless widths for the lowest $^1\Pi_u$ levels, confirming a mechanism of accidental predissociation involving the C and C' $^3\Pi_u$ states.

Rotational effects in N_2 predissociation are well known to occur for the $^1\Sigma_u^+$ states.[8–15] This is not surprising, considering the existence of allowed $^1\Pi_u \sim {}^1\Sigma_u^+$ rotational couplings and the $^1\Pi_u \sim {}^3\Pi_u$-dominated predissociation mechanism. However, apart from the J-dependent linewidths reported for $c\,^1\Pi_u(v=4)$,[11] only a few qualitative descriptions of such effects existed for other $^1\Pi_u$ states,[16] prior to the work of Stark *et al.*[1] Similarly, while rotational intensity anomalies have been reported qualitatively for some of the allowed transitions in N_2, most notably in the case of the $b\,^1\Pi_u \leftarrow X\,^1\Sigma_g^+(8,0)$ transitions of $^{14}N_2$ (Ref. 16) and $^{15}N_2$,[17] J-dependent band oscillator strengths have been measured only by Stark *et al.*[1,18]

Here, using a coupled-channel Schrödinger equation (CSE) model of the N_2 photodissociation, which includes all interactions between the b, c, and o $^1\Pi_u$ and the C and C' $^3\Pi_u$ states, we calculate the effects of rotation on the lowest-v $^1\Pi_u - X\,^1\Sigma_g^+(v,0)$ band oscillator strengths and $^1\Pi_u$ predissociation linewidths. The results are compared with the new experimental results of Stark *et al.*,[1] reported in the preceding companion paper in this issue. In addition, we report new synchrotron-based EUV photoabsorption spectra for the strongly broadened $b\,^1\Pi_u \leftarrow X\,^1\Sigma_g^+(3,0)$ transition of N_2 and perform profile analyses which reveal complex rotational variations of the band oscillator strength and $b(v=3)$ predissociation linewidth that can only be explained by

[a]Present address: Department of Chemistry, University of Wollongong, NSW 2522, Australia.
[b]Electronic mail: brenton.lewis@anu.edu.au

including in the CSE model the spin structure of the $C\,^3\Pi_u(v=9)$ state which accidentally predissociates $b\,^1\Pi_u(v=3)$.[7]

II. COMPUTATIONAL METHOD

The interactions between the Π_u states of N_2, together with the basis of the coupled-channel Schrödinger equation model of N_2 photodissociation employed here, have been described in detail in Ref. 7. Briefly, a basic five-channel diabatic model is constructed, comprising the $b\,^1\Pi_u$ valence state, $c\,^1\Pi_u$ and $o\,^1\Pi_u$ Rydberg states, and the $C\,^3\Pi_u$ and $C'\,^3\Pi_u$ valence states, coupled by mutual electrostatic interactions within the singlet and triplet manifolds and spin-orbit interactions between the manifolds. The radial Schrödinger equation for the coupled $^{1,3}\Pi_u$ states is solved numerically, yielding the coupled-channel wave functions for the excited states, which are then combined with the ground-state radial wave function and appropriate diabatic electronic transition moments, in order to form the total photodissociation cross section. By including centrifugal terms in the ground- and excited-state Hamiltonians, the rotational dependence of the cross section can be evaluated. Transition energies, rotational constants, oscillator strengths, and predissociation linewidths, deduced from the computed CSE cross sections by the fitting of Fano profiles,[19] are compared iteratively with the experimental database, in order to optimize the CSE-model parameters. Since rotational interactions with the nearby Rydberg and valence *e*-parity[20] $^1\Sigma_u^+$ states are not considered,[21] the model applies strictly only to the *f*-parity sublevels of the $^1\Pi_u$ states and Λ doubling is not treated. Therefore, except where stated otherwise, comparisons with experiment are made for *Q*-branch transitions which terminate on the *f*-parity sublevels of the excited $^1\Pi_u$ states.

The CSE model employed here differs from that of Ref. 7 in a number of respects. First, by fitting to the experimental rotationless $^1\Pi_u \leftarrow X\,^1\Sigma_g^+(v,0)$ oscillator strengths of Stark *et al.*,[1] we have been able to determine model diabatic electronic transition moments for the $b-X$, $c-X$, and $o-X$ transitions. Second, by refitting the five-channel model to the experimental energy and linewidth database used in Ref. 7, but omitting $b(v=3)$ for $^{14}N_2$ from the fit because of its local perturbation, we have obtained significantly improved model performance in this region. Third, and most importantly, in the full nine-channel CSE model used to obtain most of the results presented here, we have included specifically the spin components of the $^3\Pi_u$ states, and their **S**-uncoupling interactions,[20] assuming a diagonal spin-orbit constant $A=0\ \mathrm{cm}^{-1}$ for the C' state,[22] but allowing A for the C state, which is responsible for the accidental predissociation of the $^1\Pi_u$ states,[7] to be an adjustable parameter.

III. EXPERIMENTAL METHOD AND ANALYSIS

The photoabsorption measurements of the $b-X(3,0)$ band reported here were carried out at the 2.5 GeV storage ring of the Photon Factory, a synchrotron radiation facility at the High Energy Accelerator Research Organization in Tsukuba, Japan. The experimental procedures are detailed in Ref. 1. Briefly, a 6.65 m spectrometer with a focal plane scanner was used to provide an instrumental resolving power of $\sim 1.5\times10^5$. The spectrometer tank, at a temperature of 295 K, served as an absorption cell with a path length of 12.46 m. Absorption spectra were recorded at tank pressures ranging from 1.0×10^{-5} to 1.2×10^{-4} torr, corresponding to N_2 column densities ranging from 4.1×10^{14} to $5.0\times10^{15}\ \mathrm{cm}^{-2}$. A flowing gas configuration was used. The spectrometer tank was continuously pumped by a $1500\ \mathrm{l\,s}^{-1}$ turbomolecular pump, while N_2 entered the tank through a needle valve. The $b-X(3,0)$ band was scanned, in three overlapping portions, at a speed of $0.015\ \mathrm{nm\,min}^{-1}$; a signal integration time of about 1 s resulted in one data point for each 2.5×10^{-4} nm of the spectrum. Signal rates from the detector, a windowless solar-blind photomultiplier tube with a CsI-coated photocathode, were about 50 000 Hz for the background continuum; the detector dark count rate was less than 2 Hz. The experimental absorption spectra, which were calibrated to a precision of $\sim 0.3\ \mathrm{cm}^{-1}$ using the wave numbers of Yoshino,[23] were converted into effective photoabsorption cross sections using the Beer-Lambert law. Nonstatistical uncertainties in the cross section are estimated to be $\sim 10\%$, with contributions from the N_2 column density, the signal background, and stray light.

Due to the strong predissociation of the $b(v=3)$ level, together with overlapping of the $P(J'')$ and $Q(J''+2)$ branches for most J'' in the $b-X(3,0)$ band,[16] there are few isolated rotational lines which enable easy determination of oscillator strength and predissociation linewidth. We analyzed the experimental band cross section using a least-squares-fitting procedure in which each line was represented by a Voigt profile, with a line oscillator strength that was a parameter of the fit, a Gaussian component defined by the room-temperature Doppler width of $0.24\ \mathrm{cm}^{-1}$ full width at half maximum (FWHM), and a Lorentzian component where the width was a free parameter corresponding to the predissociation linewidth. Allowance was made for a background cross-section term with up to a quadratic dependence on wave number. The instrumental function was defined by a Voigt profile with Gaussian and Lorentzian width components of 0.60 and $0.20\ \mathrm{cm}^{-1}$ FWHM, respectively, determined by analyzing scans over the almost pure Doppler lines from the $c'\,^1\Sigma_u^+ \leftarrow X\,^1\Sigma_g^+(0,0)$ band.[18] The Voigt-model cross section was convolved, in the transmission domain, with the instrumental function, and compared iteratively with the experimental cross section. In the case of the overlapped *P* and *Q* line pairs, generally the line-strength ratios were fixed[24] and the individual line centers and predissociation widths were determined by the fit, but sometimes it was only possible to meaningfully determine an average width for the overlapped lines. In the more difficult bandhead region, where there was multiple overlapping, line-strength ratios were fixed and an optimum rotational constant for the $b(v=3)$ state was determined iteratively, enabling average predissociation linewidths to be determined for discrete regions of the spectrum. The fitted line oscillator strengths were converted into equivalent band oscillator strengths[25] by dividing by appropriately normalized $^1\Pi-{}^1\Sigma$ Hönl-London factors and fractional ground-state populations, the latter determined from $T=295$ K Boltzmann factors based on the N_2 ground-

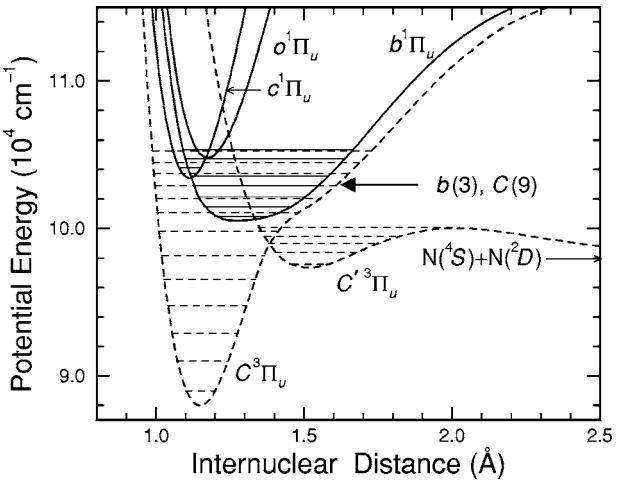

FIG. 1. Diabatic potential-energy curves used in the CSE predissociation model, on an energy scale referred to the $v=0$, $J=0$ level of the $X\,^1\Sigma_g^+$ ground state (not shown). Solid curves: $^1\Pi_u$ states. Dashed curves: $^3\Pi_u$ states. Vibrational levels for the coupled states are also indicated, located in the potential wells appropriate to their dominant character. Solid lines: $^1\Pi_u$ levels. Dashed lines: $^3\Pi_u$ levels. The degeneracy between $b(v=3)$ and $C(v=9)$ is highlighted by a solid arrow.

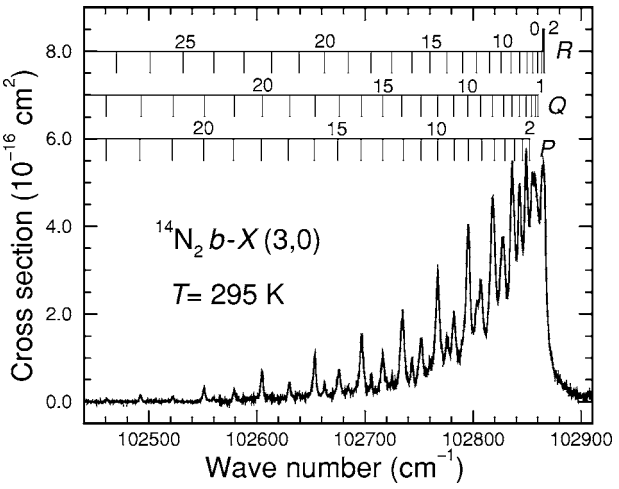

FIG. 2. Experimental room-temperature photoabsorption cross section for the $b-X(3,0)$ band of N_2, together with rotational line assignments.

state term values,[26] and taking into account the 2:1 rotational intensity alternation caused by nuclear-spin effects.

IV. RESULTS AND DISCUSSION

A. CSE-model parameters

The diabatic $^1\Pi_u$ and $^3\Pi_u$ potential-energy curves determined by least-squares fitting the five-channel CSE model to the experimental spectroscopic and linewidth database, shown in Fig. 1, differ only marginally from those of Ref. 7. This is to be expected, since similar experimental data have been employed in each case, the main differences being the omission here of the $b(v=3)$ spectroscopic data from the fit, as discussed in Sec. II, and the use of the $b(v=2)$ width data of Stark *et al.*,[1] and the present $b(v=3)$ width data. In the nine-channel model, as implied in Sec. II, the $C'\,^3\Pi_{u2}$ and $C'\,^3\Pi_{u0}$ potentials are taken as identical to the $C'\,^3\Pi_{u1}$ potential of Fig. 1 ($A=0$ cm^{-1}), while the $C\,^3\Pi_{u2}$ and $C\,^3\Pi_{u0}$ potentials are taken to differ in energy by ± 15 cm^{-1}, respectively, from the $C\,^3\Pi_{u1}$ potential of Fig. 1 ($A=15$ cm^{-1}, as discussed in Sec. IV C).

The diabatic coupling elements for the five-channel CSE model, principally sensitive to the $^1\Pi_u$ spectroscopic fitting, are also similar to those of Ref. 7. The singlet electrostatic couplings, $H_{bc}^{\rm el}$, $H_{bo}^{\rm el}$, and $H_{co}^{\rm el}$ ($\Omega=1$; $\Delta\Omega=0$), assumed to have the same relative dependences on internuclear distance R as the recommended couplings of Spelsberg and Meyer,[3] are 100%, 88%, and 98%, respectively, of those of Ref. 3. The triplet electrostatic coupling, principally sensitive to the $^3\Pi_u$ spectroscopic fitting, is $H_{CC'}^{\rm el}=790$ cm^{-1}, assumed to be R independent, with the same value adopted between all components ($\Omega=0,1,2$; $\Delta\Omega=0$) of these states in the nine-channel model. The model spin-orbit couplings, principally sensitive to the $^1\Pi_u$ linewidth fitting, are $H_{bC}^{\rm so}=46$ cm^{-1} and $H_{bC'}^{\rm so}=-1.7$ cm^{-1} ($\Omega=1$; $\Delta\Omega=0$), assumed to be R independent. In the nine-channel model, for both the C and C' states, rotational coupling (**S** uncoupling; $\Delta\Omega=\pm 1$) between the $^3\Pi_{u\Omega}$ substates is introduced in the form[20]

$$H^{JS}(\Omega,\Omega+1)=-\sqrt{2}B(R)\sqrt{J(J+1)-\Omega(\Omega+1)}, \qquad (1)$$

where $B(R)=\hbar/(2\mu R^2)$ cm^{-1}, μ is the reduced molecular mass, and $\Omega=0$ or 1.

By fitting the CSE model to the rotationless oscillator strengths of Stark *et al.*,[1] we have also determined model diabatic electronic transition moments, assuming linear dependences on R, $M_{bX}=-0.477-0.059R$, $M_{cX}=-0.655+0.377R$, and $M_{oX}=-0.035+0.401R$, all in a.u. and valid only in the narrow region of 1.05 Å$\lesssim R\lesssim$1.20 Å. At $R=1.13$ Å, these moments are 85%, 81%, and 90%, respectively, of those of Spelsberg and Meyer.[3] While the R dependences of the Rydberg electronic transition moments M_{cX} and M_{oX} are in very good agreement with those of Ref. 3, the model valence electronic transition moment M_{bX} exhibits

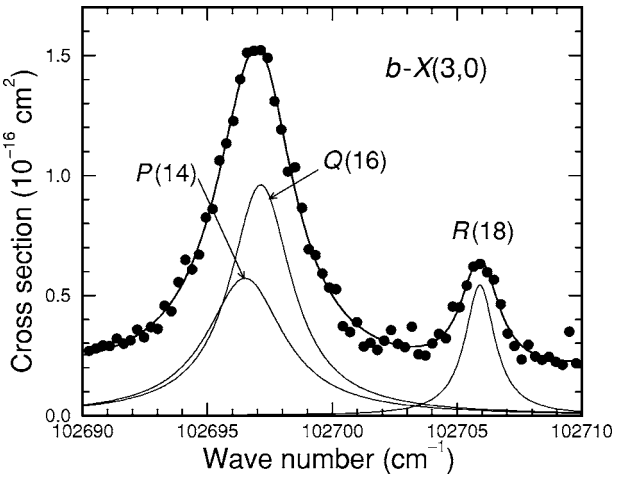

FIG. 3. Example Voigt-profile fit (thick curve) to the experimental $b-X(3,0)$ photoabsorption cross section (solid circles) near 102 700 cm^{-1}. The individual contributions (thin curves, excluding background and the effects of instrumental degradation) were obtained by fixing the $P(14)/Q(16)$ strength ratio at 1.34, yielding a fitted energy separation of 0.6(3) cm^{-1} and predissociation linewidths of 3.8(7) and 3.0(2) cm^{-1}, respectively, for the $P(14)$ and $Q(16)$ lines.

TABLE I. Experimental predissociation widths for the $b\,^1\Pi_u(v=3,J)$ levels of $^{14}N_2$, in cm^{-1} FWHM. Uncertainties, given in parentheses, in units of the least significant figure, are 1σ statistical values returned by the fit and do not include any systematic errors which may occur due to the fixing of fit parameters or instrument-function uncertainties.

J	Γ_e[a]	Γ_f[b]	Γ_{av}
2		3.40(15)[c]	3.40(15)
3	3.49(10)[d]		3.49(10)
4		3.26(7)[c]	3.26(7)
5	3.89(14)[d]	3.49(12)[c]	3.66(10)
6		3.67(8)[c]	3.67(8)
7	3.96(15)[d]	4.06(11)[c]	4.03(9)
8	4.00(14)[d]	4.08(8)[c]	4.06(7)
9	4.22(13)[d]	4.15(19)[c]	4.20(11)
10	3.99(16)[d]	3.99(8)[c]	3.99(8)
11	3.65(29)[d]	4.00(14)[c]	3.95(13)
12	3.58(24)[d]	4.22(13)[c]	4.07(12)
13	4.05(27)[e]	3.99(16)[c]	4.01(14)
14	3.26(25)[e]	3.65(29)[c]	3.42(19)
15	2.85(15)[f]	3.58(24)[c]	3.05(13)
16	2.51(29)[f]	2.98(21)[g]	2.81(17)
17	2.01(14)[f]	1.88(10)[g]	1.92(9)
18	1.75(33)[f]	1.79(9)[g]	1.79(9)
19	1.71(14)[f]	1.53(17)[g]	1.64(11)
20	1.80(24)[f]	1.39(12)[g]	1.47(11)
21	1.39(13)[f]	1.39(25)[g]	1.39(11)
22	0.98(25)[h]	1.69(14)[g]	1.51(13)
23	1.34(43)	1.26(31)[g]	1.29(26)
24	0.60(33)	1.36(19)[g]	1.17(17)
25		0.97(45)[c]	0.97(45)

[a]e-parity width from weighted mean of P- and R-branch values.
[b]f-parity width from Q-branch line.
[c]Mean width from overlapped line.
[d]Mean P or R width from overlapped lines.
[e]Individual width from overlapped P; R shoulder.
[f]Individual width from overlapped P; R resolved.
[g]Individual width from overlapped line.
[h]Mean width from overlapped P; R resolved.

significantly less dependence on R than the *ab initio* moment.[3] Considering the small range of validity of the present M_{bX}, this discrepancy is not a concern. In the future, it may be possible to clarify the R dependence of an empirical M_{bX} over a greater range by fitting to a significantly expanded experimental oscillator-strength database.

B. Experiment

A composite experimental room-temperature photoabsorption cross section for the $b-X(3,0)$ band of N_2, comprising several scans taken with different column densities, is shown in Fig. 2, together with rotational line assignments. A high degree of predissociation broadening and consequent line overlapping is evident. Therefore, the cross section is essentially absolute, except for the narrower, highest-rotational lines which are influenced somewhat by the resolution of the present experiment. The results of a Voigt-profile fit to a region of the spectrum containing overlapped P- and Q-branch lines are shown in Fig. 3. In this, as in many other cases, fixing the line-strength ratio for the overlapped lines enabled their individual predissociation widths and energy separation to be meaningfully determined.

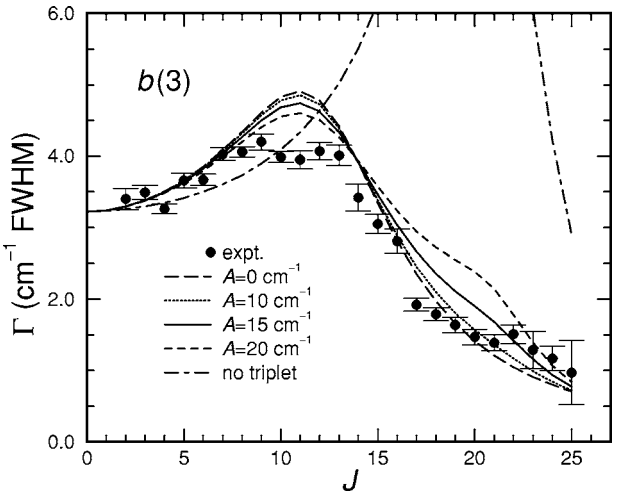

FIG. 4. Rotational variation of the $b(v=3)$ predissociation linewidth Γ. The experimental results (solid circles, weighted average values from Table I) are compared with various CSE-model calculations (curves) for the cases of a C state having no spin-triplet structure and a range of spin-orbit constants A.

The predissociation linewidths determined using the Voigt-profile fitting procedure are given in Table I and summarized in Fig. 4 (solid circles). No statistically significant e/f-parity[20] dependence of the predissociation was detected, with P-, R- and Q-branch lines terminating on levels with a common J (e and f parities, respectively) having similar widths [root mean square (rms) and maximum $e-f$ differences 1.4σ and 2.5σ, respectively]. Therefore, in order to minimize scatter, the weighted-mean e/f-parity experimental linewidths (Γ_{av} of Table I) are shown in Fig. 4. There is a very significant rotational dependence of the $b(v=3)$ predissociation, as evident from Fig. 4, with the width increasing from around 3 cm^{-1} FWHM at low J, to a maximum of around 4 cm^{-1} FWHM near $J=11$, and then falling rapidly to around 1 cm^{-1} FWHM at $J=25$. Previous estimates of linewidths in the $b-X(3,0)$ band of N_2 have varied widely, yielding values from 2.7 (Ref. 27) to 21 cm^{-1} FWHM,[28] and information on the rotational dependence has been restricted to qualitative comments indicating some narrowing at higher-J values.[16,27–29] A rough extrapolation of the present results implies a rotationless $b(v=3)$ width of about 3.2 cm^{-1} FWHM.

Equivalent $b-X(3,0)$ band oscillator strengths determined simultaneously using the Voigt-profile fitting procedure are given in Table II and summarized in Fig. 5 (solid circles). There are no statistically significant differences between the Q-branch and mean (P,R)-branch oscillator strengths for rotational lines terminating on levels with a common J (rms and maximum differences 0.9σ and 1.7σ, respectively). Therefore, the weighted-mean $(P,R)/Q$ oscillator strengths (f_{av} of Table II) are shown in Fig. 5. It is clear from Fig. 5 that the equivalent band oscillator strength decreases by about 30% as J increases from 5 to 25. This is the first documentation of this effect in the $b-X(3,0)$ band of N_2, since previous experimentally based oscillator-strength determinations have been restricted to band integrations. Not surprisingly, the present results are consistent with the inte-

TABLE II. Experimental equivalent band oscillator strengths for the $b\ ^1\Pi_u(v=3,J)\leftarrow X\ ^1\Sigma_g^+(v''=0,J'')$ transitions of $^{14}N_2$. Uncertainties, given in parentheses, in units of the least significant figure, are 1σ statistical values returned by the fit and do not include any systematic errors which may occur due to the fixing of fit parameters or N_2 column-density uncertainties.

J	f_{PR}[a]	f_Q[b]	f_{av}
4		0.042(1)	0.042(1)
5	0.042(2)[c]	0.042(2)	0.042(2)
6		0.041(1)	0.041(1)
7	0.042(1)[c]	0.042(1)	0.042(1)
8	0.035(2)[c]	0.040(1)	0.039(1)
9	0.037(2)[c]	0.040(2)	0.039(2)
10	0.037(2)[c]	0.037(1)	0.037(1)
11	0.035(2)[c]	0.035(2)	0.035(2)
12	0.039(3)[c]	0.037(2)	0.038(2)
13	0.036(2)[d]	0.037(2)	0.036(2)
14	0.032(2)[d]	0.035(2)	0.034(2)
15	0.031(1)[e]	0.039(3)	0.031(1)
16	0.030(2)[e]	0.035(2)	0.033(2)
17	0.030(2)[e]	0.032(2)	0.031(2)
18	0.031(3)[e]	0.030(1)	0.030(1)
19	0.033(2)[e]	0.030(2)	0.032(2)
20	0.031(3)[e]	0.028(2)	0.029(2)
21	0.033(2)[e]	0.032(3)	0.033(2)
22	0.028(4)[e]	0.034(2)	0.033(2)
23	0.026(6)	0.029(3)	0.028(3)
24	0.034(9)	0.033(2)	0.033(2)
25		0.025(5)	0.025(5)

[a]Weighted mean of P- and R-branch values.
[b]Mean Q-branch values from overlapped lines.
[c]Mean P- or R-branch value from overlapped lines.
[d]P overlapped; R shoulder.
[e]P overlapped; R resolved.

grated oscillator strength of 0.043(6) reported in the companion paper, Ref. 1, which is 15%–20% lower than the most recent integrated optical and electron-energy-loss values of 0.051(5) (Ref. 30) and 0.053(5),[31] respectively, i.e., marginally consistent once the combined uncertainties are considered.

TABLE III. Rotational line assignments and wave numbers for the $b\ ^1\Pi_u \leftarrow X\ ^1\Sigma_g^+(3,0)$ band of $^{14}N_2$, in cm^{-1}.

J''	$P(J'')$	$Q(J'')$	$R(J'')$
0			102 864.2[a]
1		102 860.2[a]	102 865.8[a]
2	102 852.4[a]	102 857.7[a]	102 866.2[a]
3	102 846.0[a]	102 853.9[a]	102 865.4[a]
4	102 838.3[a]	102 849.0[a]	102 863.4[a]
5	102 829.5[a]	102 842.8[a]	102 859.9[a]
6	102 819.6[a]	102 836.1[a]	102 855.4[a]
7	102 808.1[a]	102 828.0[a]	102 850.0[a]
8	102 795.8[a]	102 817.9[a]	102 843.1[a]
9	102 782.9	102 806.9[a]	102 835.1[a]
10	102 767.3[b]	102 795.2[a]	102 825.9
11	102 751.9[b]	102 782.0	102 815.4[a]
12	102 735.4	102 767.3[b]	102 803.2
13	102 716.5[b]	102 751.9[b]	102 790.5
14	102 696.5	102 734.1	102 775.9
15	102 674.8	102 716.5[b]	102 760.2
16	102 652.9	102 697.1	102 743.6
17	102 629.4	102 676.3	102 724.9
18	102 604.1	102 653.9	102 705.9
19	102 578.5	102 630.4	102 684.4
20	102 550.7	102 605.1	102 662.6
21	102 521.8	102 579.5	102 638.9
22	102 491.9	102 551.6	102 613.7
23		102 522.7	102 588.2
24		102 493.0	102 560.1

[a]Approximate value determined iteratively in whole-of-bandhead modeling.
[b]$P(J'')-Q(J''+2)$ separation unable to be determined.

The Voigt-profile fitting procedure has also allowed the determination of individual line centers for many blended features. Line-center wave numbers are given in Table III, and the corresponding $P(J'')-Q(J''+2)$ splittings are shown in Fig. 6 (solid circles), contrasted with the unresolved splittings of Carroll and Collins[16] (long-dashed line). Evidently, the broad, overlapped P and Q lines in the $b-X(3,0)$ band mask actual splittings of up to $\pm 1\ cm^{-1}$. Improved spectro-

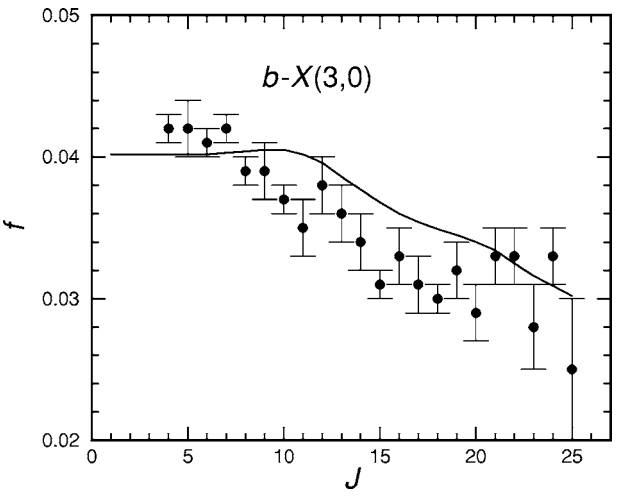

FIG. 5. Rotational variation of the $b-X(3,0)Q$-branch equivalent band oscillator strength f. The experimental results (solid circles, weighted average values from Table II) are compared with CSE-model calculations (solid curve) for $A_C=15\ cm^{-1}$.

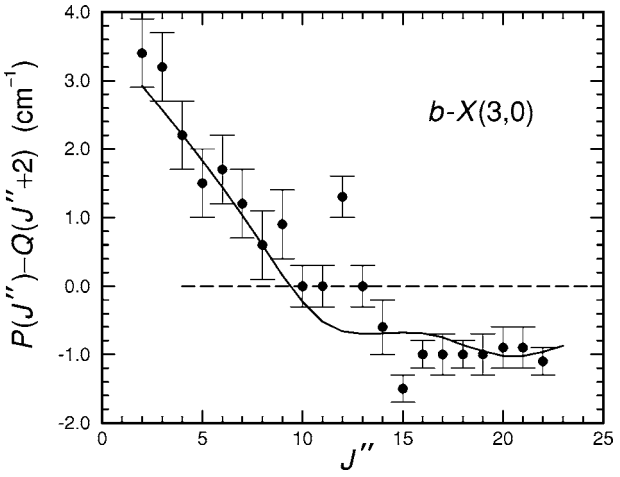

FIG. 6. Rotational variation of the splitting between the overlapped P and Q branches in the $b-X(3,0)$ band. The experimental results (solid circles) are compared with CSE-model calculations (solid curve) for $A_C=15\ cm^{-1}$. The dashed line represents the zero splitting assumed in the determination of the spectroscopic constants of Ref. 16.

TABLE IV. Spectroscopic parameters for the $b\,^1\Pi_u(v=3)$ state of $^{14}N_2$, in cm^{-1}.

Param.	Expt.	CSE[a]
ν_0	102 861.2(3)	102 860.93(5)
B	1.395(2)	1.3954(8)
D	$4.4(6)\times10^{-5}$	$4.6(4)\times10^{-5}$
H	$10(7)\times10^{-9}$	$12(4)\times10^{-9}$
q	−0.0003(3)	0[b]

[a]Uncertainties in the model spectroscopic parameters arise because the chosen polynomial order is insufficient to describe the term values precisely for this perturbed level.
[b]Fixed. Λ doubling not included in CSE model.

scopic parameters determined for the $b(v=3)$ level using the wave numbers in Table III, together with appropriate wave numbers for rotational levels of the ground state,[26] are shown in the second column of Table IV. Presumably because of the close interaction between the $b(v=3)$ and $C(v=9)$ levels, three rotational parameters are necessary to best fit the rotational terms to within $\pm0.5\ cm^{-1}$, the statistical uncertainty level. There is, perhaps, a very small degree of Λ doubling in the $b(v=3)$ level of $^{14}N_2$, Table IV indicating that $q=-0.0003(3)$, the sign expected for perturbation by a higher-lying $^1\Sigma_u^+$ state. Sprengers *et al.*[17] have reported a value $q=-0.000\,72(14)$ for the case of the $b(v=3)$ level of $^{15}N_2$.

C. Computations

Predissociation linewidths calculated using the five-channel CSE model, i.e., treating the C and C' perturbers as *singlets*, are shown in Fig. 4 as a dot-dashed curve. Clearly, as foreshadowed in Ref. 7, this model is incapable of reproducing the experimental rotational variation in the $b(v=3)$ predissociation linewidth, the calculated width increasing strongly to a maximum near $J=20$, corresponding to the crossing point between $b(v=3)$ and the higher-lying, broad $C(v=9)$, which has a smaller rotational constant. On the other hand, when the triplet structure of the C and C' states is included, leading to the nine-channel CSE model, much better agreement with experiment is obtained. Predissociation linewidths calculated using the nine-channel CSE model, for four different values of the C-state spin-orbit constant A, are also shown in Fig. 4 (other curves). Each of these curves shows qualitative agreement with experiment, the computed widths now increasing to a maximum near $J=11$, before falling precipitously. The small discrepancies between the experimental and computed values near the maximum are not of concern, once it is realized that the experimental widths in this region have been derived principally from blended features and the error bars in Fig. 4 are statistical only, not including any additional uncertainties associated with the fixing of parameters in order to cope with the blends. Although there is not great precision in the estimation of A, one can say that $A\lesssim20\ cm^{-1}$, i.e., much less than the value $A=39\ cm^{-1}$ which applies in the case of $C(v=0)$.[32] We adopt the value $A\approx15\ cm^{-1}$ (solid curve), largely on the basis that the experimental widths seem to plateau near $J=20$, roughly in agreement with the shoulder in this region of the computed curve for this value of A. This shoulder corresponds to the crossing of $b\,^1\Pi_u(v=3)$ by $C\,^3\Pi_{u1}(v=9)$, the central triplet component, while the behavior of the computed linewidth at intermediate J values must be related to the crossing by the lower component $C\,^3\Pi_{u0}(v=9)$. In summary, the **S**-uncoupled triplet structure of the strongly predissociated $C(v=9)$ level acts to severely modify its interaction with the close-lying $b(v=3)$ level, with major effects on the computed rotational variation of the predissociation linewidth. Therefore, hereafter in this work, we present for comparison with experiment only results computed using the nine-channel CSE model with $A=15\ cm^{-1}$.

$b-X(3,0)$ band oscillator strengths computed with this model, shown in Fig. 5 as a solid curve, are also in good overall agreement with the experimental results. As in the case of the linewidths, the computed oscillator strengths display J-dependent structures related to the $b(v=3)\sim C(v=9)$ crossings, but these structures are much weaker than the linewidth structures and could not be verified experimentally due to the scatter in the measurements.

Similarly, the computed values for the $b-X(3,0)P(J'')-Q(J''+2)$ splittings, shown as a solid curve in Fig. 6, are in good agreement with the experimental values. We have also determined $b(v=3)$ spectroscopic parameters from the computed term values, shown in the third column of Table IV, which are in excellent agreement with the experimentally based parameters, but we repeat that the CSE model does not include Σ states, so the effects of Λ doubling will not be evident. Some explanation is also required regarding the uncertainties given in Table IV for the *computed* parameters. Of course, the computed term values have no scatter, but there are residual *systematic* discrepancies between the computed and fitted terms, on the order of $\pm0.2\ cm^{-1}$, which are impossible to remove without using a higher-order polynomial. This, presumably, results from irregularities due to the close perturbation between $b(v=3)$ and $C(v=9)$.

Predissociation widths computed using the nine-channel CSE model are shown in Fig. 7 (solid curves) for the $b\,^1\Pi_u(v=0-2,4-6)$ and $c\,^1\Pi_u(v=0)$ levels. The computed widths display a wide range of J dependences, increasing significantly with J for $b(v=0,1,6)$, decreasing significantly for $b(v=2,5)$ and $c(v=0)$, while little J dependence is predicted for $b(v=4)$. In the two cases where comparison with experiment is possible, $b(v=2,4)$, excellent agreement is found between the computed J dependences and the experimental results of Stark *et al.*[1] (solid circles). For completeness, the low-J experimental predissociation linewidths[4,5] used to develop our N_2 predissociation model[7] are also shown in Fig. 7 (open symbols), arbitrarily assigned to $J=3$. While it is, therefore, not surprising that they are also in excellent agreement with our computed values, it should be noted that there are no further free parameters in the CSE model which would allow adjustment of the rotational dependences. Therefore, the good agreement with the experimental *rotational* widths[1] verifies the predictive power of the CSE predissociation model.

Equivalent Q-branch ($J=J''$) band oscillator strengths computed using the nine-channel CSE model are shown in Figs. 8 and 9 for the $b\,^1\Pi_u(v=0-2,4-8)\leftarrow X\,^1\Sigma_g^+(v=0)$,

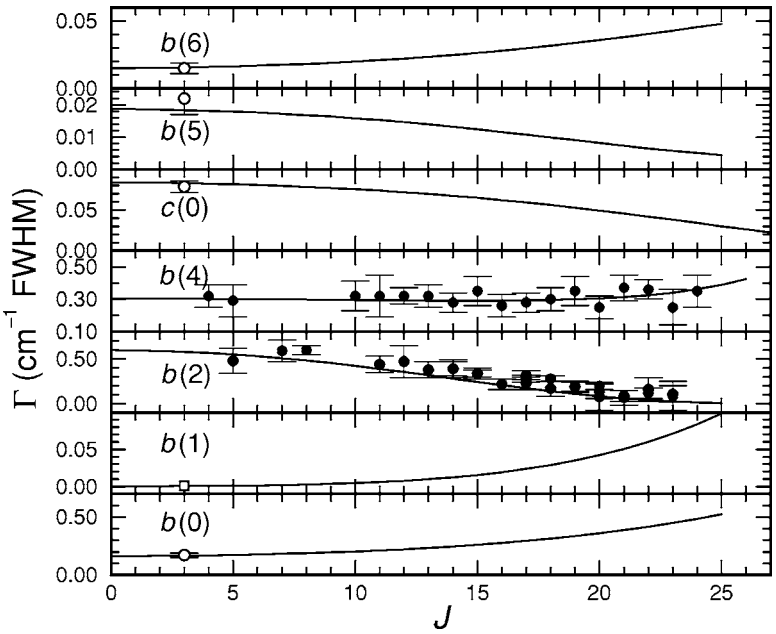

FIG. 7. Rotational variation of predissociation linewidths for $b(v=0-2,4-6)$ and $c(v=0)$. The f-parity CSE-model calculations (solid curves) are compared with experimental results from Ref. 1 (solid circles), Ref. 4 (open circles), and Ref. 5 (open square). In the case of $b(v=2)$, a level unaffected by interactions with $^1\Sigma_u^+$ states, both f- and e-parity experimental widths from Ref. 1 are shown to maximize the range of J covered.

$c\ ^1\Pi_u(v=0,1)\leftarrow X\ ^1\Sigma_g^+(v=0)$, and $o\ ^1\Pi_u(v=0)\leftarrow X\ ^1\Sigma_g^+(v=0)$ bands (solid curves). The oscillator strengths display a wide range of J dependences, increasing with J for $b-X(5,0)$, $c-X(0,0)$, and $o-X(0,0)$, decreasing for $b-X(0-2,0),(4,0),(6-7,0)$, and varying little for $c-X(1,0)$. In the case of $b-X(8,0)$, the computed rotational variation is enormous, the oscillator strength decreasing from 0.0005 at low J to $<10^{-5}$ for $J=12$ and 13, then increasing to 0.013 at $J=26$. This extreme behavior is consistent with qualitative observations from spectroscopic plates,[1,16] where the $Q(12)$ and $Q(13)$ lines from the $b-X(8,0)$ band are the only ones too weak to be observed. The very strong rotational variations in oscillator strength for the $^1\Pi_u\leftarrow X\ ^1\Sigma_g^+$ transitions are not surprising, considering that it is well known that the vibronic oscillator strengths vary erratically due to very large quantum-interference effects between the diabatic transition amplitudes, caused by the strong electrostatic couplings within the Rydberg-valence $^1\Pi_u$ manifold.[2,3,20] In particular, the $b-X(8,0)$ oscillator strength in $^{14}N_2$ is weak because of a nearly complete destructive

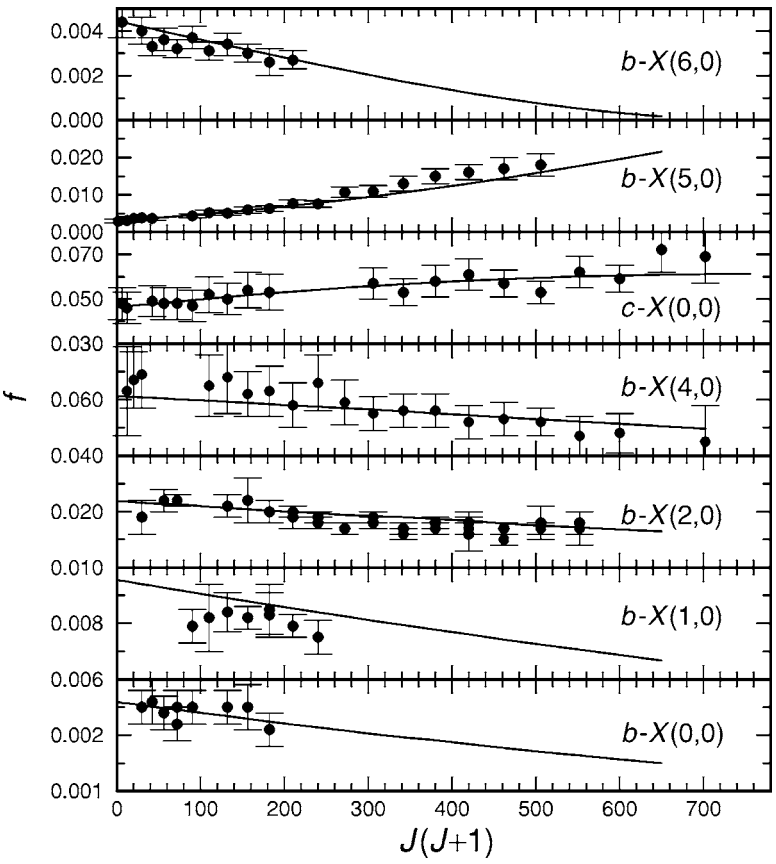

FIG. 8. Rotational variation of Q-branch equivalent band oscillator strengths f for the $b(v=0-2,4-6)\leftarrow X(v=0)$ and $c(v=0)\leftarrow X(v=0)$ transitions of $^{14}N_2$. The CSE-model calculations (solid curves) are compared with experimental results from Ref. 1 (solid circles). In the case of the $b-X(0-2,0)$ bands, which are free of P/R intensity anomalies, P-, Q-, and R-branch experimental data from Ref. 1 are shown to maximize the range of J covered.

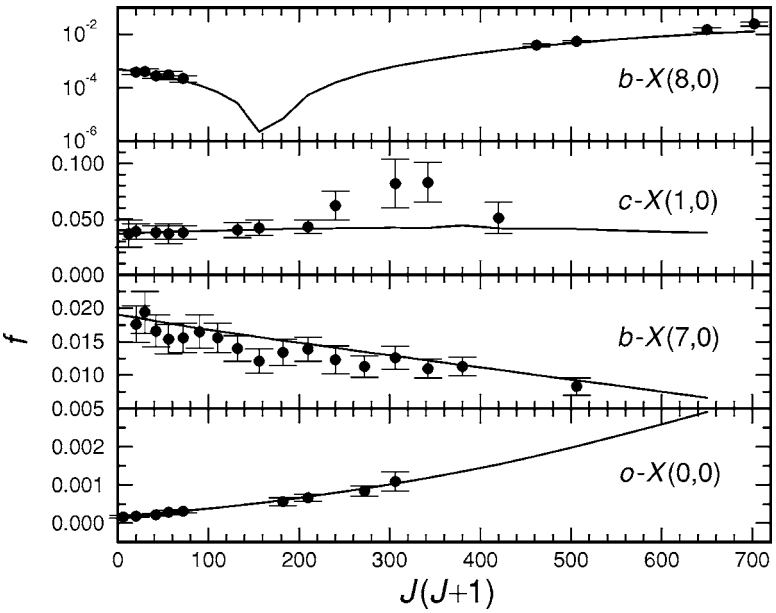

FIG. 9. Rotational variation of Q-branch equivalent band oscillator strengths f for the $b(v=7,8)\leftarrow X(v=0)$, $o(v=0)\leftarrow X(v=0)$, and $c(v=1)\leftarrow X(v=0)$ transitions of $^{14}N_2$. The CSE-model calculations (solid curves) are compared with experimental results from Ref. 1 (solid circles).

interference effect, which, evidently, becomes complete near $J=12-13$. Therefore, it is expected that, away from this cancellation point, the oscillator strength will increase rapidly, in a relative sense, for only small changes in J.

For all of the bands, the computed oscillator strengths are in excellent agreement with the experimental results of Stark *et al.*[1] (solid circles in Figs. 8 and 9), with the exception of two small areas: $c-X(1,0)$, near $J=18$, and $b-X(8,0)$, $J=25-26$, where the experimental values significantly exceed the computed values. Both of these areas lie quite high in energy, above 107 000 cm^{-1}, a little above the $F\,^3\Pi_u(v=1)$ Rydberg level,[33] which has a larger rotational constant and is likely to interact locally with both $c(v=1)$ and $b(v=8)$, possibly resulting in local oscillator-strength perturbations. Since the $^3\Pi_u$ Rydberg states, the first members of which are $3p\pi_u G\,^3\Pi_u[N_2^+(X\,^2\Sigma_g^+)]$ and $3s\sigma_g F\,^3\Pi_u[N_2^+(A\,^2\Pi_u)]$, are not included as yet in the CSE model, their effects are absent from the computed oscillator strengths; indeed, we are presently unable to extend the predissociation linewidth calculations beyond $b(v=6)$ because of the same model limitation. Nevertheless, the predictive power of the CSE model is also evident in the case of the oscillator strengths; the model diabatic electronic transition moments were optimized using only the $J=0$ extrapolated oscillator strengths of Ref. 1, yet, with no further free parameters, the rotational dependences for these *eleven* bands are reproduced in detail by the model, except for the two local effects discussed above.

V. SUMMARY AND CONCLUSIONS

A coupled-channel Schrödinger equation model of N_2 photodissociation, which includes the effects of all interactions between the b, c, and $o\,^1\Pi_u$ and the C and $C'\,^3\Pi_u$ states, has been employed to study the effects of rotation on the lowest-$v\,^1\Pi_u\leftarrow X\,^1\Sigma_g^+(v,0)$ band oscillator strengths and $^1\Pi_u$ predissociation linewidths. Analysis of synchrotron-derived EUV photoabsorption spectra of the key $b\,^1\Pi_u\leftarrow X\,^1\Sigma_g^+(3,0)$ transition of N_2 reveals that the $b(v=3)$ predissociation linewidth peaks near $J=11$, a behavior that can be explained only if the triplet structure of the C state is included explicitly in the CSE-model calculations, with a spin-orbit constant $A\approx 15$ cm^{-1} for the diffuse $C(v=9)$ level which accidentally predissociates $b(v=3)$. Predissociation linewidths and oscillator strengths calculated using this nine-channel CSE model are found to exhibit a wide range of significant rotational variations, in excellent agreement with recent experimental data, presented in a companion paper.[1] The complex rotational behavior of the $b-X(3,0)$ and other bands may be important to the modeling of EUV transmission through nitrogen-rich planetary atmospheres.

ACKNOWLEDGMENTS

This work was partially supported by Australian Research Council Discovery Program Grant No. DP0558962 and NASA Grant Nos. NAG5-9059 and NNG05GA03G. The experiments were carried out under the approval of the Photon Factory Advisory Committee (proposal 1998G245).

[1] G. Stark, K. P. Huber, K. Yoshino, P. L. Smith, and K. Ito, J. Chem. Phys. **123**, 214303 (2005), preceding paper.
[2] D. Stahel, M. Leoni, and K. Dressler, J. Chem. Phys. **79**, 2541 (1983).
[3] D. Spelsberg and W. Meyer, J. Chem. Phys. **115**, 6438 (2001).
[4] J. P. Sprengers, W. Ubachs, and K. G. H. Baldwin, J. Chem. Phys. **122**, 144301 (2005).
[5] J. P. Sprengers, W. Ubachs, A. Johansson, A. L'Huillier, C.-G. Wahlström, R. Lang, B. R. Lewis, and S. T. Gibson, J. Chem. Phys. **120**, 8973 (2004).
[6] J. P. Sprengers, A. Johansson, A. L'Huillier, C.-G. Wahlström, B. R. Lewis, and W. Ubachs, Chem. Phys. Lett. **389**, 348 (2004).
[7] B. R. Lewis, S. T. Gibson, W. Zhang, H. Lefebvre-Brion, and J.-M. Robbe, J. Chem. Phys. **122**, 144302 (2005).
[8] J. M. Ajello, G. K. James, B. O. Franklin, and D. E. Shemansky, Phys. Rev. A **40**, 3524 (1989).
[9] W. Ubachs, R. Lang, I. Velchev, W.-Ü. L. Tchang-Brillet, A. Johansson, Z. X. Li, V. Lokhnygin, and C.-G. Wahlström, Chem. Phys. **270**, 215 (2001).
[10] C. W. Walter, P. C. Cosby, and H. Helm, J. Chem. Phys. **112**, 4621 (2000).
[11] H. Helm, I. Hazell, and N. Bjerre, Phys. Rev. A **48**, 2762 (1993).
[12] J. M. Ajello, G. K. James, and M. Ciocca, J. Phys. B **31**, 2437 (1998).

[13] D. E. Shemansky, I. Kanik, and J. M. Ajello, Astrophys. J. **452**, 480 (1995).
[14] X. Liu, D. E. Shemansky, M. Ciocca, I. Kanik, and J. M. Ajello, Astrophys. J. **623**, 579 (2005).
[15] S. A. Edwards, W.-Ü. L. Tchang-Brillet, J.-Y. Roncin, F. Launay, and F. Rostas, Planet. Space Sci. **43**, 67 (1995).
[16] P. K. Carroll and C. P. Collins, Can. J. Phys. **47**, 563 (1969).
[17] J. P. Sprengers, W. Ubachs, K. G. H. Baldwin, B. R. Lewis, and W.-Ü. L. Tchang-Brillet, J. Chem. Phys. **119**, 3160 (2003).
[18] G. Stark, K. P. Huber, K. Yoshino, M. C. Chan, T. Matsui, P. L. Smith, and K. Ito, Astrophys. J. **531**, 321 (2000).
[19] Small line-shape asymmetries indicated for some computed resonances are not reported here due to the lack of possibility of experimental verification.
[20] H. Lefebvre-Brion and R. W. Field, *The Spectra and Dynamics of Diatomic Molecules* (Elsevier, Amsterdam, 2004), pp. 138–148, 212–217, and 380–403.
[21] The *f*-parity sublevels of the $^1\Pi_u$ states may be influenced by rotational interactions with $^1\Sigma_u^-$ states, also excluded from the model. There are no Rydberg states of this symmetry, but local perturbations due to high-lying levels of the $a'\ ^1\Sigma_u^-$ state cannot be excluded.
[22] P. K. Carroll, Proc. R. Soc. London, Ser. A **272**, 270 (1962).
[23] K. Yoshino (private communication); Harvard-Smithsonian Center for Astrophysics Molecular database; http://cfa-www.harvard.edu/amdata/ampdata/N2ARCHIVE/n2archive.html
[24] Initially, the strength ratios were set using appropriate room-temperature Boltzmann factors and $^1\Pi-{}^1\Sigma$ Hönl-London factors. These ratios were then adjusted iteratively to take account of the the actual *J* dependence of the oscillator strength revealed by the analysis. No P/R intensity anomalies (Ref. 20) due to $^1\Pi\sim{}^1\Sigma$ interactions were detected in this low-lying band.
[25] B. R. Lewis, L. Berzins, and J. H. Carver, J. Quant. Spectrosc. Radiat. Transf. **36**, 209 (1986).
[26] M. L. Orlov, J. F. Ogilvie, and J. W. Nibler, J. Mol. Spectrosc. **74**, 488 (1979).
[27] J. M. Robbe, Ph.D. thesis, University of Lille, 1978.
[28] M. Leoni and K. Dressler, Z. Angew. Math. Phys. **22**, 794 (1971).
[29] W. Ubachs, L. Tashiro, and R. N. Zare, Chem. Phys. **130**, 1 (1989).
[30] G. Stark, P. L. Smith, K. P. Huber, K. Yoshino, M. H. Stevens, and K. Ito, J. Chem. Phys. **97**, 4809 (1992).
[31] W. F. Chan, G. Cooper, R. N. S. Sodhi, and C. E. Brion, Chem. Phys. **170**, 81 (1993).
[32] S. G. Tilford, J. T. Vanderslice, and P. G. Wilkinson, Astrophys. J. **142**, 1203 (1965).
[33] A. B. van der Kamp, P. C. Cosby, and W. J. van der Zande, Chem. Phys. **184**, 319 (1994).